Proceedings of ASME Turbo Expo 2023
Turbomachinery Technical Conference and Exposition
GT2023
June 26-30, 2023, Boston, Massachusetts, USA

GT2023-103665

ASSESSMENT OF PART-LOAD OPERATION STRATEGIES OF SUPERCRITICAL POWER CYCLES USING CARBON DIOXIDE MIXTURES IN CSP PLANTS, INCLUDING AIR-COOLED CONDENSER OPTIMISATION

P. Rodríguez-de Arriba, F. Crespi,* D. Sánchez, L. García-Rodríguez,
Department of Energy Engineering, University of Seville, Camino de los descubrimientos s/n, 41092 Seville, Spain

ABSTRACT

This manuscript, developed in the framework of SCARABEUS project, presents an assessment of the part-load performance of a transcritical Recompression cycle running on a 80%CO_2-20%SO_2 mixture under different load-control schemes.

The first part of the paper describes the computational platform of the integrated system, implemented in Thermoflex but with profuse use of in-house scripts, in order to accurately describe the off-design performance of key components when operating on CO_2 mixtures with non-ideal gas behaviour. These off-design models make use of performance maps for turbomachinery -provided by the SCARABEUS partners- whereas the Conductance Ratio Method employed to model the counter-current heat exchangers is calibrated with in-house tools. The paper is specifically focused on the Heat Rejection Unit, for which a specific design tool accounting for accurate heat transfer between working fluid and cooling medium (air) and for auxiliary power consumption -both in off-design- has been developed by the authors.

In the second part of the paper, different operating strategies of the power cycle are considered, based on keeping one of the following three parameters constant: turbine inlet temperature, turbine outlet temperature or return temperature of molten salts. Globally, plant operation is constrained by the need to keep the temperature of cold HTF returning to the storage system as close as possible to its rated (design) value and by the need to keep turbine outlet temperature below 450ºC to avoid the installation of an external cooling system in the low pressure section of this equipment. Therefore, the trade-off between these two parameters and system net efficiency are assessed in the paper. Regarding the Air-Cooled Condenser, the optimal operation strategy of this component found to be based on a combination of Single-speed and Variable Frequency Driver fans.

The results show that the operation at constant turbine inlet temperature leads to the highest net efficiency of the power block, closely followed by the control scheme based on constant return temperature of the heat transfer fluid. Nevertheless, this latter option enables a perfect control on the other two figures of merit. As a consequence, the identification of the best operation strategy must be addressed in future works by means of a thorough techno-economic assessment considering the annual yield of the plant.

Nomenclature

α	Split flow factor
$\dot{m}$	Mass flow rate
η	Efficiency
ACC	Air-cooled condenser
HTF	Heat transfer fluid (molten salts)
HTR	High temperature recuperator
HX	Heat exchanger
$LCoE$	Levelised cost of energy
LTR	Low temperature recuperator
MW	Molar weight
PHX	Primary heat exchanger
TIT	Turbine inlet temperature
TOT	Turbine outlet temperature
VFD	Variable Frequency Driver

*Address all correspondence to this author. Email: crespi@us.es

WF	Working fluid
Z	Compressibility factor
p.p.	Percentage point

Subscript

HR	Heat recuperator
C	Cold
cond	Condensation
cr	Critical
cricdb	Cricondenbar
d	On-design conditions
glide	Width of mixture p-T envelope for a given P_{cond}
H	Hot
HP	High-pressure side
LP	Low-pressure side
norm	Normalised
off	Off-design conditions
P	Pump
pp	Pinch-point (minimum ΔT)
RC	Recompressor
s	Isentropic
T	Turbine
th	Thermal

Introduction

It is widely believed that Concentrating Solar Power (CSP) plants will play a crucial role in the decarbonisation of the power generation sector [1]. Nevertheless, although the dispatchability of CSP (i.e., capability to deliver power on demand) is a great advantage over photovoltaic and wind power, this technology is nowadays still far from being economically viable due to its high cost of electricity (LCoE). This makes it mandatory to find routes to achieving higher solar-to-electric efficiency and to reduce the overall capital cost of CSP plants, thus improving the plant's economic performance. In this landscape, supercritical CO_2 power cycles are being extensively studied due to their potentially higher thermal efficiency, smaller footprint, lower cycle complexity and expectedly higher part-load performance than the steam Rankine cycles used in contemporary CSP plants. Unfortunately, sCO_2 cycles experience a drastic performance drop at high ambient temperatures (>35ºC) because they can no longer carry out the compression process at high density near the critical point (31ºC) [2].

The SCARABEUS project is funded by the Horizon 2020 programme of the European Commission and focuses on the development on new power block technologies, based on CO_2 mixtures, for application to CSP plants. In SCARABEUS, the addition of certain dopants to the raw working fluid (CO_2) shifts the critical temperature of the resulting mixture to a value higher than that of Carbon Dioxide, hence enabling condensation of the working fluid at higher temperatures than in conventional supercritical CO_2 power plants. The twofold benefit of this is a much lower compression work (liquid compression) and a higher potential for internal heat recovery which, altogether, brings about higher thermal efficiencies of the power block.

Several dopants have been investigated within the project - for instance C_6F_6, $TiCl_4$ or SO_2 [3, 4]- and their positive impact has already been demonstrated from a thermodynamic standpoint. In particular, it is possible to achieve cycle efficiencies of ∼45% with state-of-the-art Turbine Inlet Temperatures (TIT=550ºC) and >50% if TIT is raised to 700ºC, what is representative of current and next-generation CSP technologies [5]. This means that, in comparison with pure CO_2 technology, CO_2 blends either i) achieve higher η_{th} -if similar configurations are used-, or ii) or enable simpler cycle layouts -if similar performance is sought- [6].

Based on this past work, the present paper provides a further step in the development of the SCARABEUS concept, presenting a preliminary analysis of the part-load operation of CSP plant making use of a Recompression cycle running on 80% CO_2 - 20% SO_2. The first part of the manuscript summarises the main characteristics of the selected mixture and power cycle. In the second part, the computational platform developed for this work is presented; this has been developed using the commercial software Thermoflex and incorporating a series of in-house design tools for certain equipment that are specific to sCO_2 technology. In this part, a thorough description of the design and off-design models is provided. The third section discusses different issues related to system operation, with a special focus on the operation of the air-cooled condenser (ACC). Finally, the fourth section presents the results and main conclusions of the analysis, identifying the operating strategies that maximise net plant efficiency.

Computational Environment

The reference CSP plant considered in this paper is a central receiver (tower) plant with a two-tank molten-salt Thermal Energy Storage system (TES), which enables operation at full load without solar energy supply for 17.5 hours. The power block adopts a transcritical (condensing) Recompression cycle running on a mixture of 80% CO_2 and 20% SO_2 (molar basis). This configuration is a mere adaption of the well-known Recompression cycle running on pure Carbon Dioxide, widely investigated in literature for CSP applications [7, 8], and has already been studied by the members of the SCARABEUS consortium in previous publications [4, 9], showing superior thermal performance [5]. Due to the transcritical, condensing nature of this layout, the air-cooler and the main compressor are replaced by an air-cooled condenser and a pump, respectively, while the other cycle stations/components remain unchanged. A scheme of the cycle layout and a temperature-entropy diagram are provided in Fig. 1.

The main thermo-physical properties of the working fluid have been calculated using the commercial software Aspen Plus v12 [10], employing the Equation of State PC-SAFT. This selection is based on the theoretical and experimental work carried out by the SCARABEUS teams at Politecnico di Milano

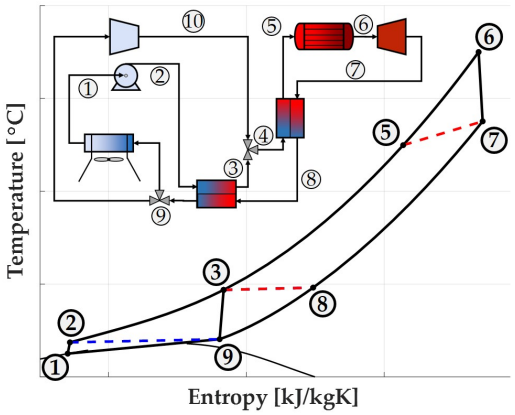

FIGURE 1: Transcritical Recompression Cycle running on 80%CO_2-20%SO_2 mixture: layout and temperature-entropy diagram

and University of Brescia, and a complete set of specifications is provided in [9]. Transport properties (i.e., thermal conductivity and dynamic viscosity) are calculated using REFPROP10 [11]. The optimum composition of the mixture for the boundary conditions considered was identified in [4], accounting for a large enough temperature gap (∼20ºC) between minimum cycle temperature (T_{min}) and critical temperature (T_{cr}). This a safety margin to ensure that the working fluid can be condensed even under extreme ambient conditions. The main characteristics of the mixture are summarised in Table 1, whilst a thorough discussion about safety hazards following standard NFPA 704 can be found in other works by the authors [4].

TABLE 1: Main characteristics of the working mixture: 80%CO_2-20%SO_2.

MW [kg/kmol]	T_{cr} [ºC]	P_{cr} [bar]
48.03	68.7	100.4
P_{cricdb} [bar]	T_{cond} [ºC]	ΔT_{glide} [ºC]
101.6	79.1	18.8

The power cycle has been modelled in the commercial software Thermoflex v.30 [12]. A series of specific performance models for all cycle main components have been added to Thermoflex by means of LUA scripts, substituting the default lumped-volume models, and the thermophysical properties of the working fluid obtained with Aspen have been incorporated via look-up tables employing the *User-defined refrigerant fluid* tool. This novel approach has been adopted for the following beneficial features: i) it enables the development of a robust calculation platform, guaranteed by the high reliability and computational robustness of the Thermoflex suite; ii) the use of specific performance models overcomes the main limitation of Thermoflex in this respect, which is the lack of specific performance models for equipment running on CO_2-based mixtures. Such in-house performance models account now for both on and off-design operation and have been obtained with specific design tools developed by various members of the SCARABEUS consortium (more information in the next section). The complete set of specifications is summarised in Table 2 for rated conditions, whilst the heat and mass balance of the reference cycle is provided in Table 3. It is to note that the specifications in Table 2 are different from those presented in previous works by the authors ([3, 4]), in particular for the isentropic efficiency of turbomachinery and the pressure drops across heat exchangers; this is due to the updated information obtained in recent theoretical and experimental work within the project. It is worth noting though that these new assumptions do not change the main outcomes of past works from a qualitative standpoint.

TABLE 2: Design point specifications of the *Recompression Cycle* running on CO_2-SO_2.

Parameter	Value	Parameter	Value
$\dot{W}_{gross}$ [MW]	100	η_{th} [%]	44.15
α [-]	0.375	TIT [ºC]	550
$P_{WF,max}$ [bar]	250	$T_{WF,min}$ [ºC]	50
$T_{HTF,H}$ [ºC]	565	$T_{HTF,C}$ [ºC]	387.8
$\eta_{T,s}$ [%]	91.9	$\eta_{RC,s}$ [%]	82.7
$\eta_{P,s}$ [%]	87.4	$\Delta T_{pp,HR}$ [ºC]	5
$\Delta T_{pp,PHX}$ [ºC]	15	$\Delta P_{WF,PHX}$ [%]	0.5
$\Delta P_{WF,ACC}$ [%]	0.5	$\Delta P_{HR,LP}$ [%]	1.5
$\Delta P_{HR,HP}$ [%]	0.25	$TES_{capacity}$ [h]	17.5
$P_{WF,min}$ [bar]	79.1	TOT [ºC]	412.2

Detailed components models

This section provides a general description of the numerical models employed to estimate the rated and off-design performance of major equipment in the cycle. These performance models, embedded in Thermoflex by means of LUA scripts, are the result of component-specific design tools, developed with different software by the SCARABEUS consortium.

Turbine. The turbine in the reference plant is a 14-stage, axial machine, whose design has been produced by City University of London and Baker Hughes using 3D CFD tools (more information in recent publications by these partners [13, 14]).

TABLE 3: Heat and mass balance. Station numbers as per Fig. 1.

Cycle station	T [ºC]	P [bar]	h [kJ/kg]	s [kJ/kgK]	$\dot{m}$ [kg/s]	Z [-]
1	50.00	79.10	-8007	-1.148	680.7	0.181
2	74.84	250.0	-7983	-1.136	680.7	0.492
3	193.5	249.4	-7755	-0.566	680.7	0.790
4	193.5	249.4	-7755	-0.566	1089.1	0.790
5	372.8	248.8	-7525	-0.147	1089.1	0.985
6	550.0	247.5	-7317	0.139	1089.1	1.042
7	412.2	81.90	-7451	0.155	1089.1	0.989
8	198.5	80.69	-7679	-0.243	1089.1	0.891
9	81.80	79.50	-7822	-0.592	1089.1	0.642
10	193.5	249.4	-7755	-0.566	408.4	0.790

The corresponding performance map introduced in Thermoflex by means of a LUA script shows isentropic head coefficient Ψ and isentropic efficiency $\eta_{T,s}$ as a function of inlet flow coefficient Φ and peripheral (blade) Mach number M_{u2}, Eq. (1). Note that these non-dimensional coefficients, see Eq. (2), consider non-ideal gas performance where $\dot{m}$ is the circulating mass flow rate (kg/s), v_{01} and a_{01} are the specific volume and speed of sound at turbine inlet (specific volume in [m^3/kg]), D is the diameter of the hub (m), N is rotational speed (rad/s) and Δh_{0s} is the isentropic enthalpy drop across the expander.

$$[\Psi, \eta_s] = f(\Phi, M_{u2}) \tag{1}$$

$$\left[\frac{\Delta h_{0s}}{a_{01}^2}, \eta_s\right] = f\left(\frac{\dot{m} \cdot v_{01}}{a_{01}^2}, \frac{N \cdot D}{a_{01}}\right) \tag{2}$$

Recompressor. The recompressor (cycle stations 9-10 in Fig. 1) has been modelled by Baker Hughes as a variable-speed, fixed-geometry axial machine (i.e., without inlet guides vanes). Following an approach widely employed in literature, a performance map has been produced to estimate isentropic head coefficient and efficiency as a function of flow coefficient and peripheral Mach number, similar to the one previously presented for the turbine in Eqs. (1,2).

Pump. A centrifugal, variable-speed pump has been specifically designed by Baker Hughes. The resulting performance map is then incorporated into Thermoflex using the PCE pump tool based on the functional relationship in Eq. (3), where H stands for pump head, ρ is density at pump inlet, ω is rotational speed, D is diameter of the pump impeller, $\eta_{P,s}$ is isentropic efficiency and $\dot{V}$ is volumetric flow rate ([m^3/s]).

$$\left[\frac{H}{\frac{1}{2}\rho(\omega \cdot D)^2}, \eta_{is}\right] = f\left(\frac{\dot{V}}{w \cdot D^3}\right) \tag{3}$$

Heat recuperators. Following an approach widely accepted in literature, Printed Circuit Heat Exchangers have been considered for the Low (LTR) and High-Temperature (HTR) Recuperators. An enhanced version of the in-house thermo-mechanical model already presented in [15] assumes semi-cylindrical straight channels. The diameter of the channels is 2 mm whilst the pitch and plate thickness are calculated to ensure mechanical integrity using the methodology proposed in [16]. The Conductance Ratio Method is implemented in Thermoflex via LUA scripts to estimate the performance in rated conditions and in off-design operation. This method, originally developed and validated in [17, 18] and then extensively used in literature [8], allows to estimate the performance of a HX as a function of the overall thermal conductance ($U \cdot A$) and the ratio of the two $h \cdot A$'s, $(h \cdot A)_{ratio}$ in Eq. (4). The first metric is obtained in Thermoflex, considering the specific boundary conditions of the heat exchanger, whilst the second one is calculated with the aforementioned design model applied to both recuperators. The resulting values are provided in Table 4.

For off-design performance, $h \cdot A$'s are obtained through scaling of the corresponding design values. Scaling factors accounting for variations of thermal conductivity, Reynolds and Prandtl numbers are provided in Eq. (5), where the values of exponent y are 0.3 on the hot side and 0.4 on the cold side, according to Dittus-Boelter's correlation. The complete methodology can be found in past work by the authors [17, 18]. Off-design pressure drops are calculated from the corresponding rated values with Eq. (6), where ρ is the density of the fluid. All properties have been evaluated at the average temperature and pressure between inlet and outlet, on each side.

$$(h \cdot A)_{ratio} = \frac{(h \cdot A)_{hot,d}}{(h \cdot A)_{cold,d}} \tag{4}$$

$$(h \cdot A)_{off} = (h \cdot A)_d \left(\frac{k_{off}}{k_d}\right) \left(\frac{\dot{m}_{off}/\mu_{off}}{\dot{m}_d/\mu_d}\right)^{0.8} \left(\frac{Pr_{off}}{Pr_d}\right)^y \tag{5}$$

$$\Delta P_{off} = \Delta P_d \left(\frac{\dot{m}_{off}}{\dot{m}_d}\right)^2 \left(\frac{\rho_d}{\rho_{off}}\right) \tag{6}$$

Primary heat exchangers. The primary heat exchanger taking the working fluid to the target temperature at turbine inlet is of the shell-and-tube type, with two passes in the shell. The working fluid flows across the tubes, whilst nitrate molten salts are on the shell side. This component is modelled using the default *shell-tube general HX* item provided by Thermoflex. For

the reference plant, the resulting PHX has a shell diameter of 4.6 m, 26582 tubes with length 19.2 m, an outlet tube diameter of 19.05 mm and a tube wall thickness of 4.25 mm. The tubes are arranged in a staggered layout (45º rotation).

It is to note that the *shell-tube general HX* item in Thermoflex is not available for *User-defined refrigerant fluid* -the one employed to model the performance of the power cycle- so the *Air specified by composition* fluid specification has been used instead. For this reason, the design of the PHX is carried out in a separate Thermoflex file, and the corresponding performance is incorporated into the power cycle platform by means of the Conductance Ratio Method (see previous section). Note that the Conductance Ratio Method works well with shell-and-tube HXs, as already demonstrated in past works by the authors; yet, the exponents in Eq. (5), on the molten salts side, have been updated following Bell-Delaware's correlation instead of Dittus-Boelter's. Now, 0.604 is used rather than 0.8, and exponent $y = 0.33$. Equation (6) is used to calculate off-design pressure drops.

TABLE 4: Conductance ratio values for LTR, HTR and PHX

	LTR	HTR	PHX
$(\mathbf{h}\cdot\mathbf{A})_{\mathbf{ratio}}$	1.059	0.875	1.794

Heat rejection unit. Identifying the best configuration of a large-scale CO_2 cooler is not trivial, and clear indications cannot be found in literature. The same applies to CO_2-based mixtures, which present the added difficulty of multi-species condensation. In this study, the technology of choice is a horizontal, direct air-cooled condenser (ACC), following the design proposed by Kelvion Thermal Solutions, the industrial partner of SCARABEUS responsible for heat exchangers. In the proposed ACC, the working mixture flows inside horizontal, finned tubes arranged in three vertical passes with a staggered distribution, whereas cooling air flows vertically upwards using induced-draft axial fans. The heat transfer model of the tube bundle was presented originally by Illyés *et al.* [19] and validated against data provided by Kelvion. Based on this, the methodology for the detailed complete design of this modular ACC was presented by the authors in [20], including an in-house axial fan design tool.

The ACC tool is developed in Matlab, and run separately from the Thermoflex model since, for a set value of the internal pressure drop, the design of the cooling unit does not really affect the gross thermal performance of the power cycle. The tool calculates the number of bays, number of tubes per bay, number of fans per bay and their design-point efficiency, and total fan power consumption, among others parameters. Trade-offs between component size and fan power consumption were studied, obtaining reasonable designs whose main specifications are provided in Table 5; all the parameters in this table are in line with common practice.

TABLE 5: Air-cooled condenser specifications

Parameter	Value	Parameter	Value
Tube length [m]	18	Number of bays	19
Air face velocity [m/s]	3	Fans per bay	3
Fan diameter [m]	5.18	Tubes per bay	94
Fan arrangement	induced	External area [m^2]	399043
Fan efficiency [%]	69.2	U [W/m^2K]	21.56
Motor efficiency [%]	98	$\dot{W}_{ACC}$ [kW]	1115

Off-design performance is also calculated by means of the aforementioned in-house code. To this end, two different types of fans are considered: single speed (on/off) and variable speed. Each bay of the modular ACC can include a combination of single and variable speed fans to account for different heat duties when operating in off-design conditions. A discussion about the possible arrangements and operating strategies is included in the next section.

System operating strategies and constraints

In this section, different system operating strategies are presented, together with the main operational constraints set by the safe operation of the components of the power block.

Following the most common approach in literature, the main control scheme is based on inventory, which is applied in combination with sliding turbine inlet pressure. The pump and compressor are operated at variable speed to ensure a wide enough operating range. Additionally, it is acknowledged that recirculation might be needed to avoid compressor surge but, in the scope of this analysis, this is not needed since the compressor runs far from the surge line in any operating condition. The split-flow factor is kept constant and equal to its design value, see Table 2, since this is found to have only a limited effect on cycle performance. It is noted that the design of the inventory tank and the modelling of the mixture management system fall out of the scope of the present paper, and will be addressed in future works by the authors.

Three main part-load operating strategies are studied in this work:

- **Constant Turbine Inlet Temperature** (TIT): already proposed by Alfani *et al.* for Recompression cycles running on pure CO_2 [21], this strategy has the main benefit of maintaining a high η_{th} at part-load. As a shortcoming, when

combined with sliding pressure operation, holding TIT at the rated value brings about an increase of Turbine Outlet Temperature (TOT). This has two possible detrimental effects: i) higher capital cost because of the need to implement cooling in the last stages (or the exhaust duct) of the turbine; ii) a reduced TES capacity, produced by the smaller enthalpy drop between hot and cold tank given as a consequence of the higher return temperature to the cold tank ($T_{HTF,C}$) -caused by the higher temperature of the working fluid at the outlet from the high temperature recuperator (cycle station 5 in Fig. 1)-.

• **Constant** $T_{HTF,C}$: this strategy has been proposed by Neises in [8]. It has the main objective to avoid the decreasing TES capacity with increasing TOT when constant TIT is used. It also aims to alleviate other thermo-mechanical problems in the receiver. In order to achieve constant $T_{HTF,C}$, TIT must be reduced at partial load, with a consequent performance drop (i.e., lower η_{th}).

• **Constant** TOT: this strategy aims to control the temperature at turbine outlet in order to avoid the need for cooling in the low-pressure section of the turbine. Akin to the constant $T_{HTF,C}$ case, this comes at the expense of reducing TIT and, thus, η_{th}. An upper limit of turbine outlet temperature is set to 450ºC, as suggested by the industrial partner of SCARABEUS responsible for this equipment. Thus, this strategy replaces any of the other two above whenever $TOT > 450$ºC, what, in this work, happens at loads lower than 60% in combination with constant TIT.

In addition to the high-level control rules described above, the following operational constraints are considered: i) maximum cycle pressure is limited to 250 bar, common value in literature [8]; ii) this maximum pressure cannot, on the other hand, be lower than the cricondenbar pressure (101.6 bar), in order to prevent supercritical evaporation inside the recuperators during the heating of the mixture; iii) in order to avoid condensation (of any of the species in the mixture) at the inlet to the Recompressor, the temperature at this station must be higher than the dew temperature for the corresponding inlet pressure[1]; iv) the power consumption of the ACC can exceed its rated value by up to 5%, in order to accommodate slight variations in the operating point of the fans due to air density changes while the fans run at the rated speed.

The proposed operating strategies are analysed when the heat input to the power cycle is reduced with respect to the rated value, with the final aim to identify which control scheme yields higher net power output. Although the focus is on net thermal performance, and given that this analysis is a mandatory first step towards the complete techno-economic optimisation of SCARABEUS concept, other aspects such as the utilisation of the inventory of molten salts in the TES system or the avoidance of higher capital costs if turbine cooling in the exhaust section were eventually needed will also be discussed.

Gross (η_{th}) and net (η^*_{net}) efficiencies are defined in Eqs. (7,8). $\dot{Q}_{PHX}$ is the heat input to the power cycle (provided by the HTF delivered by the TES system), $\dot{W}_T$ stands for turbine expansion power, whilst $\dot{W}_P$ and $\dot{W}_{RC}$ are the power consumed by the pump and compressor respectively. In addition to mechanical losses, accounted for by the corresponding mechanical efficiencies (η_m, all set to 0.98), two main contributions to auxiliary power consumption are taken into account in the definition of η^*_{net}: fan power consumption of the ACC ($\dot{W}_{ACC}$) and molten salt (circulation) pump providing HTF to the Primary Heat Exchanger ($\dot{W}_{HTF}$). ACC fan power is calculated as the sum of the power consumed by all the ACC fans in operation. The power consumed by the circulation pump of molten salts, $\dot{W}_{HTF}$, is computed with Eq. (9), accounting for the pressure loss taking place across the PHX (ΔP_{PHX}), the pressure head needed to overcome the height of the cold tank (set to 12.2m, according to [22]) and the absolute pressure of the cold tank (10^5Pa, according to [23]).

The authors acknowledge that this definition of net efficiency is not exhaustive since there are other contributions to auxiliary power consumption not accounted for in η^*_{net}; for instance, tracking system of the heliostats in the solar field, or high-pressure pump delivering molten salts to the receiver. Nevertheless, the definition presented in Eq. (8) takes into consideration all the effects that are needed to assess which the optimal operating strategy of power block and ACC is. The contribution of other items will be considered in future works, to carry out a complete techno-economic analysis of the system.

$$\eta_{th} = \frac{\dot{W}_T - \dot{W}_P - \dot{W}_{RC}}{\dot{Q}_{PHX}} \tag{7}$$

$$\eta^*_{net} = \frac{\dot{W}_T \eta_{T,m} - \dot{W}_P/\eta_{P,m} - \dot{W}_{RC}/\eta_{RC,m} - \dot{W}_{ACC} - \dot{W}_{HTF}}{\dot{Q}_{PHX}} \tag{8}$$

$$\dot{W}_{HTF} = \frac{\dot{m}_{HTF}}{\rho_{HTF,H} \cdot \eta_{P,s} \cdot \eta_{P,m}} (\Delta P_{PHX} + g \cdot \rho_{HTF,H} \cdot H_{tank} + P_{tank}) \tag{9}$$

Optimum operating strategy of the Air Cooled Condenser

The Air Cooled Condenser is one of most significant contributions to auxiliary power consumption in a CSP plant. For this reason, an accurate estimate of this contribution is of utmost importance, along with the identification of the optimum operating

[1] Several works on supercritical CO_2 radial compressors have reported that this equipment can run with liquid CO_2 in the inducer. Therefore, this can be considered as a weak constraint which might be lifted if needed. Nevertheless, despite considering it initially, it is found that these conditions are never met for the cases of interest (loads higher than 50%), thus no compressor operations with liquid inlet are taken into account in the present paper.

strategy of the ACC yielding minimum power consumption for higher plant performance.

In this section, different part-load operating strategies of the ACC are discussed, assuming that condensation pressure $P_{WF,min}$ remains constant at the rated value (see Table 2); this implies that the condensation (bubble) temperature of the working fluid is constant also. Once the optimum ACC operating strategy is identified for the boundary conditions of interest, the corresponding $\dot{W}_{ACC}$ is calculated and used to estimate η^*_{net} according to Eq.(8).

It is worth noting that, in order to simplify the numerical scheme of the solver, the temperature of the mixture at the inlet to the ACC is assumed to be constant, meaning that the heat duty of the ACC ($\dot{Q}_{ACC}$) is proportional to the circulating mass flow rate of working fluid ($\dot{m}_{WF}$). This is a conservative assumption since, as observed in the next section, $\dot{Q}_{ACC}$ tends to decrease in partial load; i.e., in practice, the actual $\dot{Q}_{ACC}$ for a given $\dot{m}_{WF}$ is lower than estimated in this study. This assumption has nevertheless a small effect on the estimated ACC performance, since the sensible heat duty (i.e., the fraction of $\dot{Q}_{ACC}$ being rejected prior to condensation) is less than 15% of the total $\dot{Q}_{ACC}$.

The flexibility of the ACC during part-load operation depends on the number of bays (multiplicity) and on the number of fans incorporating variable frequency drive (VFD) in each bay (i.e., the number of fan that can be operated at variable speed). Three cases are considered: bays with 3 single speed (i.e., on/off) fans, without VFD (*Bay1*); bays with 2 single-speed fans and 1 variable-speed fan (*Bay2*); and bays with all 3 fans with VFD (*Bay3*). These three scenarios allow the assessment of trade-offs between capital and operational costs of the ACC, since increasing the number of VFD fans leads to a reduction in fan power consumption, but at the expense of higher installation costs. With the aim to provide a preliminary economic analysis, Table 6 shows the breakdown of capital cost for each type of bay, estimated according to data from industrial partners in the SCARABEUS consortium and considering two main contributions: tube bundles and fans. Since all bays have the same tube bundles, this contribution is the same for the three cases (around 236 k€ per bay). As for fans, those with VFDs are roughly 60% more expensive than single-speed ones. Accordingly, the total capital cost of *Bay2* and *Bay3* are 3% and 8.4% higher than *Bay1*, respectively.

TABLE 6: Breakdown of CapEx for each bay (tube bundles and fans) and total cost per bay and for the entire ACC. All costs expressed in k€.

Bay type	Tube bundles	Fans	Single bay	ACC
Bay1 (w/o VFD)	236	40.0	276	5242
Bay2 (1 VFD)	236	47.7	284	5390
Bay3 (3 VFD)	236	63.1	299	5682

The operation of a single bay is discussed in first place. Fig.2(a) represents, in solid grey lines, the trend of the minimum temperature of the working fluid temperature $T_{WF,min}$ as a function of normalised mass flow rate ($\dot{m}_{WF,norm}$) for various combinations of fans in operation and/or at a reduced rotating speed. This information about fan operation is provided in brackets as [w_1 w_2 w_3], where w_i represents the rotational speed of each fan in the bay normalised with respect to the rated value. Accordingly, 1 would indicate that the fan is running at design speed, 0 that the fan is not in operation and any number between 0 and 1 represents a fan with VFD running at reduced speed[2]. Values of $T_{WF,min}$ below 50ºC in Fig.2(a) represent an operating condition where condensation has occurred.

Figure2(b) shows fan power consumption (normalised to the design value) for the same cases as in Fig.2(a). The operation of the three scenarios considered is plotted on these two figures. *Bay1* is represented in solid black line, *Bay2* in dashed black line, whilst *Bay3* in dotted-dash black line. For the *Bay1* case, Fig. 2(b) shows that all three fans must be in operation in order to ensure condensation if $\dot{m}_{WF,norm} > 60\%$ (line [1 1 1]). At lower duties, one of the fans can be shut down whilst still ensuring condensation of the working fluid (vertical drop to line [0 1 1]); this enables $\sim 33\%$ lower $\dot{W}_{fan,norm}$. Finally, a second fan can be put off-service for heat duties lower than 25% of the rated value (vertical drop to line [0 0 1]), enabling another an additional 33% $\dot{W}_{fan,norm}$ reduction with respect to the design value.

A similar scenario is depicted in Fig. 2(a), where two step-changes of $T_{WF,min}$ to higher values can be observed in correspondence with the shutdown of each fan, followed by a progressive reduction of working fluid temperature. For the *Bay2* case, replacing one single-speed fan with one with VFD enables controlling $T_{WF,min}$ so that condensation of the working fluid can be ensured for any $\dot{m}_{WF,norm}$ without excursions into the sub-cooled liquid region (horizontal line in Fig. 2(a)). This means that $\dot{W}_{fan,norm}$ can also be drastically reduced with respect to *Bay1*.

In Fig. 2(b), the *Bay2* case exhibits an overall $\dot{W}_{fan,norm}$ pattern similar to that provided by *Bay1*, but with significantly smoother reductions from line to line. Finally, the *Bay3* case ensures the lowest $\dot{W}_{fan,norm}$ (dotted-and-dash line) inasmuch as all the fans incorporate VFD (hence avoiding the parasitic power consumption of the two single-speed fans in *Bay2*). Akin to the *Bay2* scenario, $T_{WF,min}$ can be controlled for any $\dot{m}_{WF,norm}$ even though the horizontal line cannot be seen in Fig. 2(a) because it is covered by the line for *Bay2*.

The performance of the condenser of the reference SCARABEUS plant, comprised of 19 bays, for the three aforecited cases/scenarios is discussed now. Figure 3(a) shows the different ACC operational profiles, where $\dot{m}_{WF,norm}$ refers to the

[2]In Fig.2, only lines corresponding to 0, 0.5 or 1 are provided in order to increase readability. Any other off-design fan speed could have been considered though.

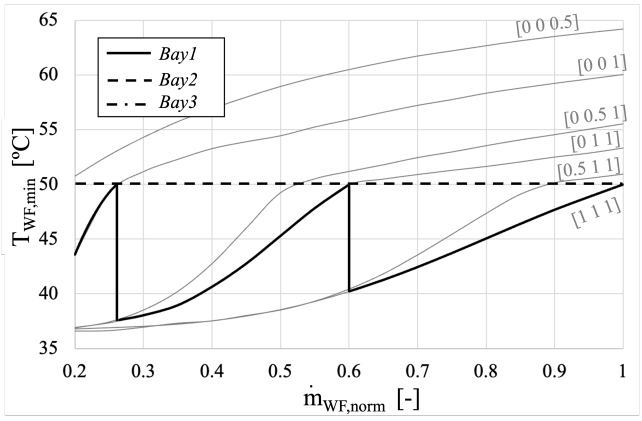

(a) Working fluid temperature at ACC outlet as a function of $\dot{m}_{WF,norm}$. The *Bay3* case is not seen because it is completely overlapped by *Bay2*.

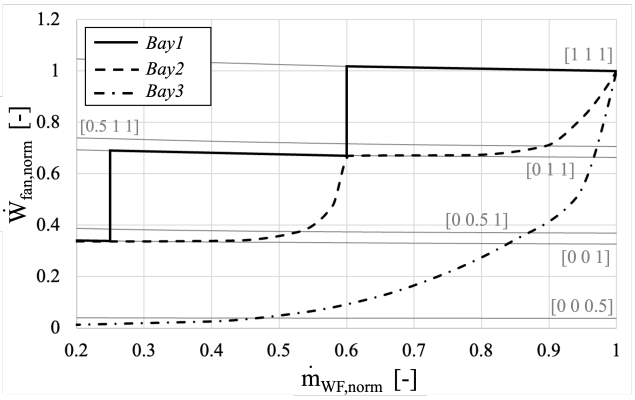

(b) Normalised fan power consumption as a function of $\dot{m}_{WF,norm}$.

FIGURE 2: $T_{WF,min}$ and $\dot{W}_{fan,norm}$ as a function of $\dot{m}_{WF,norm}$ per bay. Different bay operating strategies are shown.

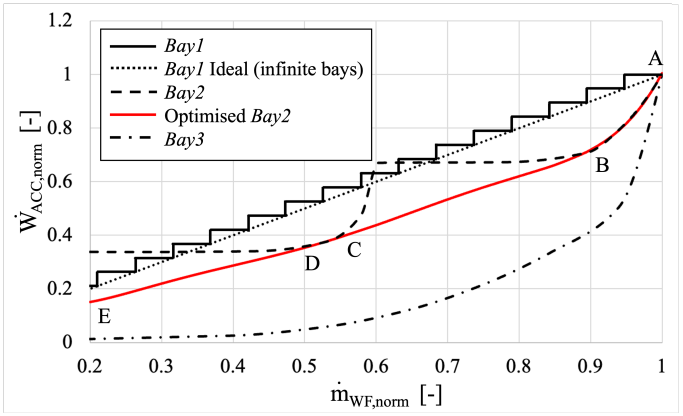

(a) $\dot{W}_{ACC,norm}$ as a function of $\dot{m}_{WF,norm}$. Different ACC operating strategies are shown.

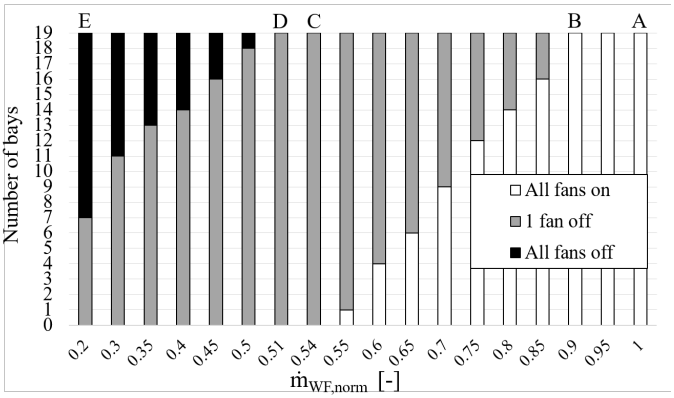

(b) Number of bays in each operating condition as a function of $\dot{m}_{WF,norm}$. Optimised *Bay2* strategy is considered.

FIGURE 3: $\dot{W}_{ACC,norm}$ and bays operating conditions as a function of $\dot{m}_{WF,norm}$.

total mass flow rate of working fluid circulating through the ACC (not just a single bay), whilst the vertical axis represents the overall power consumption normalised with respect to the rated conditions ($\dot{W}_{ACC,norm}$).

Employing the same criterion as in Fig. 2, the black solid line in Fig. 3(a) represents the performance of the ACC when all the bays are operated according to the *Bay1* case. In this case, bays are progressively shut down as $\dot{Q}_{ACC}$ decreases, in particular when the reduction of $\dot{m}_{WF,norm}$ equals the design mass flow rate of an individual bay (nineteen steps in total). Since the number of bays is higher than the number of fans per bay, this implies a wider load control capacity. Also, the results suggest that it might be better to shut down complete bays rather than individual fans, as far as efficiency is concerned. If this scheme were adopted, the system could be controlled as shown in Fig. 3(a), where each step reduction of $\dot{W}_{ACC}$ would represent the shutdown of a single bay. It becomes evident that, the larger the number of bays, the closer this operation strategy is to the ideal case represented by the diagonal dotted line (infinite number of bays).

The dotted-and-dash line in Fig. 3(a) refers to the *Bay3* case, when all the VFD fans experience parallel speed reductions (i.e., same speed reduction for all the fans). Similarly, the dashed line represents the *Bay2* scenario, considering all the bays operating with the same combination of single-speed and VFD fans. For this reason, the trends observed for *Bay2* and *Bay3* are almost identical to those in Fig. 2(a).

The part-load performance of the condenser in case *Bay2* can nevertheless be largely improved by taking advantage of the multiplicity of the system. This is clear in Fig. 3(a) for values of $\dot{m}_{WF,norm}$ lower than $\sim$0.45 and also between $\sim$ 0.6 and $\sim$ 0.8. In these heat duty ranges, the total fan power of the air cooled condenser in case *Bay2* becomes similar to that of *Bay1* or even higher. In the light of these results, an analysis is carried out to find the optimum operating strategy for the *Bay2* scenario, making use of an optimiser based on genetic algorithms.

Two main optimisation variables are considered: $\dot{m}_{WF,norm}$ sent to each bay (with respect to the rated value) and rotational speed of the VFD fans. If $\dot{m}_{WF,norm}$ in a bay takes values lower than 0.2, then that bay is shut down and the corresponding mass flow rate is equally distributed among the remaining bays. This is an arbitrary, conservative assumption, adopted to prevent the flow velocity of working fluid circulating in pipes from dropping dramatically. Another optimisation constraints is that the sum of all of $\dot{m}_{WF,norm}$ per bay must be equal to the value of $\dot{m}_{WF,norm}$ under study, as well as neither negative nor higher than the design flow rate of the bay ($1/N_{bays}$).

The results of this optimisation are plotted in red in Fig. 3(a). In addition, Fig. 3(b) shows the operating conditions for each of the 19 bays, differentiating three scenarios: all fans in operation (white bar), one single-speed fan off (grey) and all fans off (black). From point A (100% of $\dot{m}_{WF,norm}$) to point B (90%), all bays operate with identical flow rates, having all fans in operation: single-speed fans at full speed and VFD fans running at the speed needed to control the outlet temperature of the working fluid; for instance, the rotational speed of the VFD fan in point B is around 50% of the nominal speed (see Fig. 2 (a)). From point B to point C, the bays are all in operation but now some of them have progressively turned down one single-speed fan (see Fig. 3(b)). In the bays with all fans operating, VFD fans run at the same speed as in point B, whereas the bays where one single-speed fan is not in operation have the VFD fan running at 54% the normalised mass flow rate and 60% the rated rotational speed (point C). As expected, as the operating conditions ($\dot{m}_{WF,norm}$) get closer to point C, the number of bays with just one single-speed fan in operation (in addition to the VFD fan) increases. From point C to point D (around 51% of the normalised flow rate of working fluid), all bays have one single-speed fan not in operation and are again operated identically. At point D, the rotating speed of VFD fans is 50% the rated value (see Fig. 2(a) for a $\dot{m}_{WF,norm}$ of 51%) and, for lower loads, some bays are just shut down while the rest remain operating as in point D (with one single-speed and one VFD fan).

This optimised *Bay2* scenario shows a much better performance than the standard one considered originally. It enables a 25-30% relative reduction of $\dot{W}_{ACC}$ with respect to *Bay1*, depending on the particular heat duty ($\dot{m}_{WF,norm}$). Very interestingly, this reduction is enabled by the utilisation of just one VFD per bay, what means a mere 3% increase in capital cost (see Table 6). In absolute values and for the reference plant considered, the rise in capital cost could be as high 7.7k€ per bay, or around 148k€ for the entire ACC. On the other hand, the *Bay3* case would enable relative reductions of $\dot{W}_{ACC}$ in the range from 70 to 90%, but this would be at the expense of significantly higher capital costs, since all 57 fans would be of the VFD type (in lieu of the 19 VFD fans in the optimised *Bay2* scenario). In this latter case, the resulting capital cost increase could be as high as 23.1k€ / 15.4k€ per bay (around 440k€ / 292k€ for the entire ACC) with respect to *Bay1* / *Bay2* respectively. The effects of these operating strategies and bay concepts/scenarios on cycle net efficiency are discussed in the next section.

Part-load operation of the SCARABEUS system

In order to assess the part-load performance of the entire power block, multiple simulations have been carried out with the integrated platform developed in Thermoflex. Operation at reduced loads is enabled by reducing the mass flow rate of molten salt ($\dot{m}_{HTF}$), which brings about lower $\dot{Q}_{PHX}$ and $\dot{m}_{WF}$ at constant $P_{WF,min}$ (thus, $T_{WF,min}$) and α. The results from these simulations have then been post-processed to compute the net efficiency (η^*_{net}) and net power output ($\dot{W}^*_{net}$) of the system, for each control scheme (constant TIT, $T_{HTF,C}$ or TOT) and ACC scenario (*Bay1*, *Bay2* or *Bay3*) of interest. In the following, load is expressed as a percentage of $\dot{W}^*_{net}$, ranging from 30% to 100% of the rated value (90.9 MWe, corresponding to 100 MW gross output at generator terminals).

Figure 4 compares the net efficiency (η^*_{net}) obtained employing the three different ACC operating strategies (scenarios) for constant turbine inlet temperature control in the power block. All three curves are very similar, with net efficiency peaking at around 90% load. This is in line with the results obtained by other authors [21, 8] and comes about because of the oversized capacity of the recuperators. Considering *Bay1* as the reference case, the use of one VFD fan in each bay (i.e., *Bay2*) enables 0.1 percentage points higher η^*_{net} across the entire load range whereas*Bay3* leads to a larger η^*_{net} gain of about 0.3 p.p. Though these efficiency gains might seem marginal, their impact on LCoE must be assessed before a final conclusion is made. Unfortunately, the limited length of this paper makes it not possible to present a complete discussion of this and, therefore, it will be presented in future works by the authors. Now, only *Bay2* is considering on the assumption that it likely yields the best compromise between enhanced performance and moderate capital cost increase.

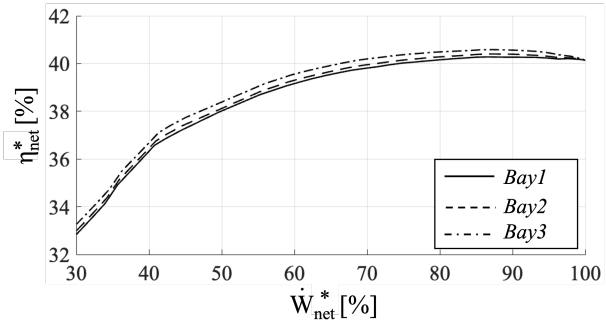

FIGURE 4: Net efficiency of the system as a function of net power output. Different ACC operating strategies are considered.

Figures 5 (a) and (b) show the gross (η_{th}) and net (η^*_{net}) efficiencies of the power block operating in partial load, for the three control schemes considered. Solid lines refer to constant TIT, dashed lines to constant $T_{HTF,C}$, and dotted-and-dash lines stand for constant TOT. It is observed that, for loads higher than 60%, the difference between the first two strategies is moderate: around 0.75 p.p. and 1.1 p.p. for η_{th} and η^*_{net} respectively. The gain achieved if constant TIT is used in partial load increases at lower loads, reaching 1.65 p.p. at 40%. Nevertheless, this gain comes at the expense of turbine outlet (exhaust) temperatures higher than 450ºC, what happens at loads lower than $\sim 60\%$ (see Fig.5(f)). To overcome this problem, a constant TOT control scheme is adopted, but this has a negative impact on efficiency since the η_{th} and η^*_{net} gains are reduced to around 0.7 p.p. Finally, Fig.5(f) also shows that, if $T_{HTF,C}$ is kept constant, rather than TIT or TOT, then TOT is always lower than 450ºC. This removes the need to incorporate cooling in the low pressure section of the turbine.

The decreasing trend of $P_{WF,max}$ in part-load conditions, caused by the use of sliding pressure at turbine inlet, is depicted in Fig. 5(c). This trend is virtually the same for all control schemes, quantitatively and qualitatively, and confirms that the minimum value of $P_{WF,max}$ ($\sim$150 bar at 30% load) is considerably higher than the cricondenbar pressure (101.6 bar, see dotted line in Fig. 5(c)). Accordingly, the risk of supercritical evaporation occurring inside the high-pressure side of the recuperators is avoided, should this be a problem for the integrity of these heat exchangers. If it were, a throttle valve at turbine inlet could be used to ensure a high enough pressure of the working fluid across the recuperators.

Regarding TIT, this parameter presents a progressive reduction when a constant $T_{HTF,C}$ scheme is adopted (see Fig. 5(d)); in particular, TIT drops down to 530ºC at 50% load and to around 510ºC at 30%. On the contrary, when constant TOT is adopted, the trend of TIT present two largely different sections: constant at loads higher than $\sim$60% and with a steeper reduction at lower loads. Figure5(e) also shows that constant TIT brings about a large increase of $T_{HTF,C}$ (hence, reduction of TES capacity), reaching 407ºC before the transition to constant TOT at $\sim$60% load. For lower loads, the former trend is partly offset by the latter effect, causing $T_{HTF,C}$ to decrease to almost its rated value. Regarding $\dot{m}_{WF}$, Fig. 5(g) shows that the three control schemes present very similar trends, with a slightly larger reduction for constant TIT. On the contrary, the mass flow rate of molten salts is significantly higher when constant TIT is used (10% higher at 60% load), as observed in Fig. 5(h). This is due to the higher $T_{HTF,C}$ when turbine inlet temperature is kept constant, what also has the effect of reducing the effective capacity of the Thermal Energy Storage system (faster consumption of the existing inventory of molten salts in the hot tank). As discussed in the previous sections, this side effect could completely offset the slightly higher efficiency of the constant TIT load control scheme, from a techno-economic standpoint (LCoE).

Finally, Fig. 5(i) depicts the inlet tempeaturature of the recompressor in part-load operation. All three control schemes exhibit very similar trends, with this temperature decreasing to values very close to the dew point of the working fluid at $\sim$50% load, below which condensation is expected to arise. This raises some concern about the actual operatibility of this component at such conditions, also due to the onset of possible internal condensation brought about by local flow accelerations. Future works will address suitable strategies to control the inlet temperature of the recompressor, possibly based on bypassing the the low-temperature recuperator or on compressor recirculation.

Last but not least, Fig. 6 illustrates the performance maps of the recompressor (a) and turbine (b). The running lines from 100% to 50% load for both constant TIT and constant $T_{HTF,C}$ control are marked with red and blue markers respectively. Both turbomachines show a safe operating path, reasonably close to the design point for a large range of operating conditions. Also, for the recompressor, the surge margin is reduced at low loads, mostly because of the fast reduction of the flow coefficient brought about by inventory control. This will have to be studied in detail in future works focused on startup manoeuvres.

Conclusions and further work

This manuscript presents an assessment of the part-load performance of a transcritical Recompression cycle running on 80% CO_2 - 20% SO_2 and using different load-control schemes, with special focus on the optimisation of Air-Cooled Condenser operation. The following conclusions are drawn:

- The use of a proper combination of two single-speed and one VFD fan in each bay leads to a $\sim$ 70% reduction of ACC power consumption with respect to the case using single-speed fans only. It is to note, though, that the incorporation of VFD comes at a cost, estimated in a 3% rise in the CapEx of the Air Cooled Condenser.
- If all fans were of the VFD type, the relative reduction would increase to 90%, but this would require significantly higher capital costs (70% more VFD fans are needed).
- More specifically, the utilisation of one VFD per bay implies 148k€ higher capital cost of the ACC, and this value increases to 440k€ if all fans are of the VFD type.
- Keeping turbine inlet temperature constant in partial load yields the highest net efficiency. On the negative side, this strategy is worst according to the other two figures of merit considered: both $T_{HTF,C}$ and TOT increase significantly, reducing the effective capacity of the TES system and setting the need for cooling in the last stages of the turbine.
- These issues can be partially overcome by adopting a hybrid control scheme using constant TIT at high loads, and constant TOT at intermediate and low loads. In the refer-

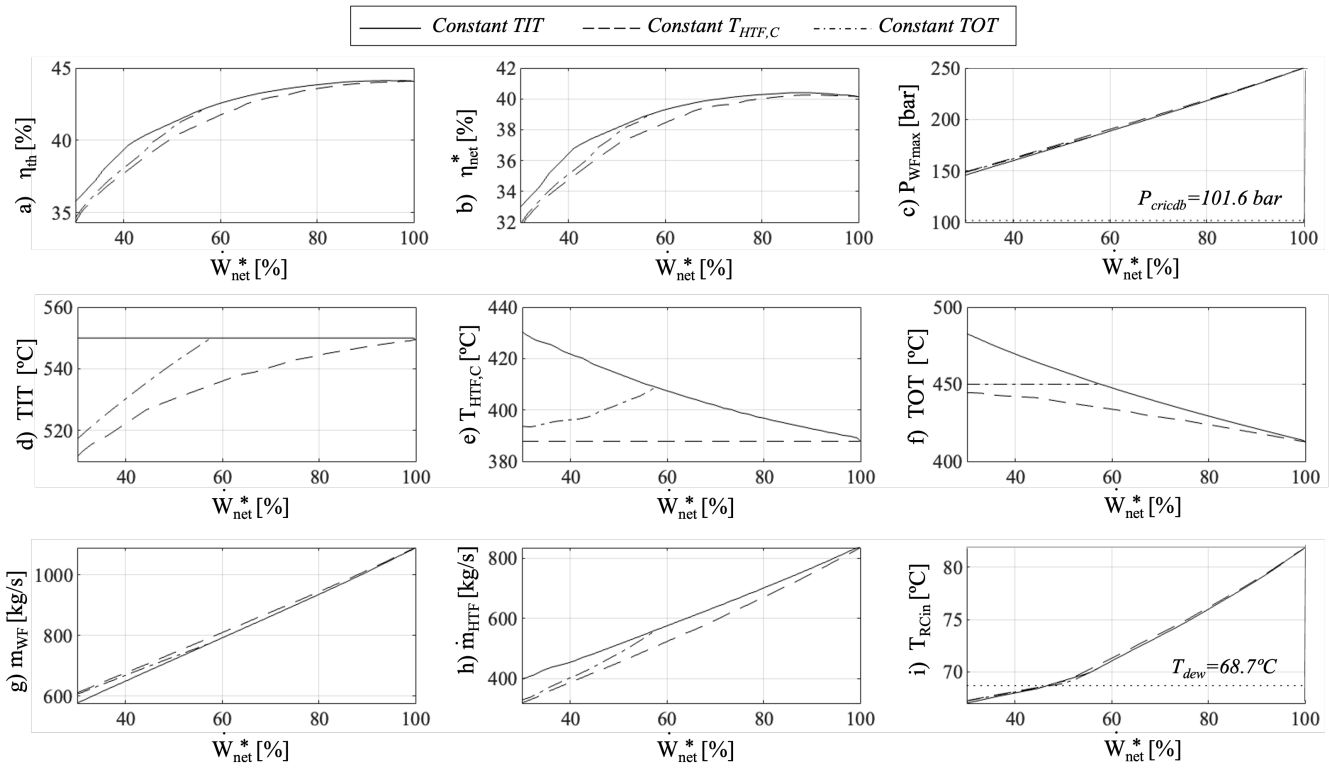

FIGURE 5: System performance (various parameters) as a function of net power output. Three control schemes of the power block are considered. Sub-figure captions are provided near the y-axis.

ence case in this work, the transition between both regimes takes place at 60% load.

- The utilisation of a control scheme based on constant $T_{HTF,C}$ yields very similar results to the combination of constant TIT/TOT at high and moderate/low loads.
- In order to define the optimal operating strategy of the overall system, a thorough techno-economic analysis must be addressed in terms of LCoE, factoring in the trade-offs between the counteracting effects described in the previous bullet points.

ACKNOWLEDGEMENTS

The SCARABEUS project has received funding from the European Union's Horizon 2020 research and innovation programme under grant agreement Nº814985.

The SCARABEUS teams at Baker-Hughes, Kelvion and City, University of London are gratefully acknowledged for their valuable discussions about operational limits of turbomachinery and heat exchangers in the power block of the reference SCARABEUS plant. The SCARABEUS team at Kelvion is gratefully acknowledged also for its valuable contribution to estimating the capital cost of Air Cooled Condenser unit.

Last but not least, the Spanish Ministry of Universities is gratefully acknowledged for sponsoring the contract of Pablo Rodríguez de Arriba via FPU (Formación de Profesorado Universitario) grant ref. FPU21/04892.

References

[1] G. Resch et al. "Deep decarbonization of the European power sector calls for dispatchable CSP". In: *AIP Conference Proceedings*. Vol. 2445. 1. AIP Publishing LLC. (2022), p. 050006.

[2] V. Dostal, M. J. Driscoll, and P. Hejzlar. "A supercritical carbon dioxide cycle for next generation nuclear reactors". In: *PhD Thesis, Massachusetts Institute of Technology, Department of Nuclear Engineering* (2004).

[3] F. Crespi et al. "Thermal efficiency gains enabled by using CO_2 mixtures in supercritical power cycles". In: *Energy* 238 (2022).

[4] F. Crespi et al. "Preliminary investigation on the adoption of CO_2-SO_2 working mixtures in a transcritical Recompression cycle". In: *Appl. Therm. Eng.* 211 (2022).

[5] P. Rodrıguez-deArriba et al. "The potential of transcritical cycles based on CO_2 mixtures: An exergy-based analysis". In: *Renew. Energ.* 199 (2022).

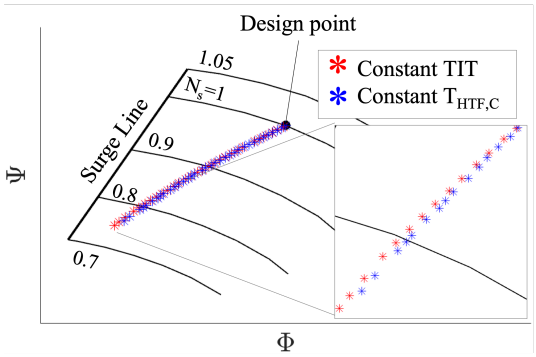

(a) Compressor.

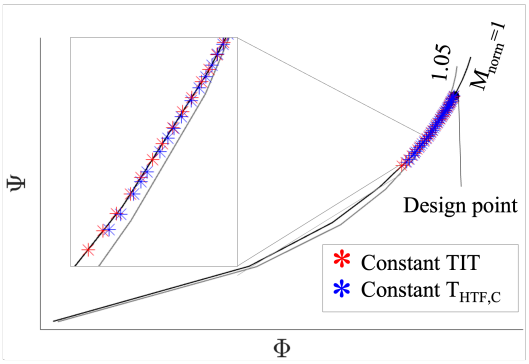

(b) Turbine

FIGURE 6: Non-dimensional performance maps of compressor and turbine, showing running lines. Two control schemes are considered.

[6] F. Crespi et al. "Influence of working fluid composition on the optimum characteristics of blended supercritical carbon dioxide cycles". In: *Turbo Expo: Power for Land, Sea, and Air*. Vol. 85048. ASME. (2021), V010T30A030.

[7] T. Neises and C. Turchi. "Supercritical carbon dioxide power cycle design and configuration optimization to minimize levelized cost of energy of molten salt power towers operating at 650 C". In: *Sol. Energy* 181 (2019).

[8] T. Neises. "Steady-state off-design modeling of the supercritical carbon dioxide recompression cycle for concentrating solar power applications with two-tank sensible-heat storage". In: *Sol. Energy* 212 (2020).

[9] E. Morosini et al. "Adoption of the CO_2+ SO_2 mixture as working fluid for transcritical cycles: A thermodynamic assessment with optimized equation of state". In: *Energ. Convers. Manage.* 255 (2022).

[10] *Aspen Plus - Leading process simulator software*. Online, accessed January 5th 2023. 2023. URL: https://www.aspentech.com/en/products/engineering/aspen-properties.

[11] E. Lemmon et al. "NIST Standard Reference Database 23: Reference Fluid Thermodynamic and Transport Properties-REFPROP, Version 10.0, National Institute of Standards and Technology". In: *Standard Reference Data Program, Gaithersburg* (2018).

[12] *Thermoflow Inc, Thermoflow suite - Thermoflex software*. Online, accessed January 5th 2023. 2023. URL: https://www.thermoflow.com/products$%5C_$generalpurpose.html.

[13] A. S. Abdeldayem, M. T. White, and A. I. Sayma. "Comparison of CFD Predictions of Supercritical Carbon Dioxide Axial Flow Turbines Using a Number of Turbulence Models". In: Turbo Expo: Power for Land, Sea, and Air. V010T30A010. (2021).

[14] A. S. Abdeldayem et al. "Integrated Aerodynamic and Structural Blade Shape Optimization of Axial Turbines Operating With Supercritical Carbon Dioxide Blended With Dopants". In: *J. Eng. Gas Turb. Pow.* 144.10 (2022).

[15] F. Crespi et al. "Capital cost assessment of concentrated solar power plants based on supercritical carbon dioxide power cycles". In: *J. Eng. Gas Turb. Pow.* 141.7 (2019).

[16] R. Le Pierres, D. Southall, and S. Osborne. "Impact of mechanical design issues on printed circuit heat exchangers". In: *Proceedings of 3rd sCO_2 Power Cycle Symposium*. (2011).

[17] K. Hoopes, D. Sánchez, and F. Crespi. "A new method for modelling off-design performance of sCO_2 heat exchangers without specifying detailed geometry". In: *Proceedings of 5th sCO_2 Power Cycles Symposium*. (2016).

[18] F. Crespi et al. "The conductance ratio method for off-design heat exchanger modeling and its impact on an sCO_2 recompression cycle". In: *Turbo Expo: Power for Land, Sea, and Air*. Vol. 50961. ASME. (2017), V009T38A025.

[19] V. Illyés et al. "Design of an Air-Cooled Condenser for CO_2-Based Mixtures: Model Development, Validation and Heat Exchange Gain with Internal Microfins". In: *Turbo Expo: Power for Land, Sea, and Air*. Vol. 86083. ASME. (2022), V009T28A016.

[20] P. Rodríguez-deArriba et al. "A methodology to design air-Cooled condensers for supercritical power cycles using carbon dioxide and carbon dioxide mixtures". In: *Proceedings of the 5th European sCO_2 Conference for Energy Systems*. (2023).

[21] D. Alfani et al. "Off-design performance of CSP plant based on supercritical CO2 cycles". In: *AIP Conference Proceedings*. Vol. 2303. 1. AIP Publishing LLC. 2020, p. 130001.

[22] M. Mehos et al. *Concentrating solar power Gen3 demonstration roadmap*. Tech. rep. National Renewable Energy Lab.(NREL), Golden, CO (United States), (2017).

[23] J. M. Rodrıguez et al. "Techno-economic assessment of thermal energy storage solutions for a 1 MWe CSP-ORC power plant". In: *Sol. Energy* 140 (2016).